Turkish Journal of Civil Engineering, 2023 111-138, Paper 735, ***Research Article***

Analysis of the Hydrodynamic Characteristics in a Rectangular Clarifier under Earthquake-Induced Sloshing

Murat AKSEL[1]

ABSTRACT

Wastewater treatment plants, which play a crucial role in protecting the hydrosphere, are earthquake-prone infrastructures with large tanks and sensitive equipment. Damage to the structures in such facilities during seismic activity on the lithosphere can cause environmental pollution and threaten public health. Since the units/tanks in the treatment plants are not of different geometries and sizes, they may exceed the freeboard of the wave height due to the sloshing event. In this study, the sloshing dynamics of a rectangular type of clarifier were investigated. First, numerical parameters, boundaries, and initial conditions were validated using the results of an experimental campaign. Secondly, model conditions were kept constant, and geometry was enlarged (i.e., scaled-up) to investigate the variation of hydrodynamic forces near vulnerable equipment (such as scrapers and weirs) in clarifier. The numerical model was run for characteristics of two different earthquakes (i.e., Chi Chi-1999 and Kocaeli-1999). The results showed that dynamic pressure values near vulnerable equipment increased up to 120 times higher than the operating conditions. The maximum sloshing wave heights were calculated as 1.2 m and 1.45 m for Chi Chi (1999) and Kocaeli (1999) earthquakes, respectively.

Keywords: Natural disasters, earthquake, treatment plant, sloshing, public and environment health.

1. INTRODUCTION

Seismic activities in the lithosphere, earthquakes, have devastating effects. Important past and recent earthquakes (e.g., Alaska 1964, Loma Prieta 1989, Kobe 1995, Kocaeli 1999, Tohoku 2011, Christchurch 2011) have damaged many civil and industrial infrastructures such as highways, airports, bridges, water transmission lines, and treatment systems, as well

Note:
- This paper was received on August 9, 2022 and accepted for publication by the Editorial Board on March 20, 2023.
- Discussions on this paper will be accepted by July 31, 2023.
- https://doi.org/10.18400/tjce.1268771

1 Alanya Alaaddin Keykubat University, Department of Civil Engineering, Antalya, Türkiye
murat.aksel@alanya.edu.tr - https://orcid.org/0000-0002-6456-4396

as residential buildings. Infrastructure facilities are critical facilities that must maintain their functionality even after an earthquake.

The earthquake has direct and indirect impacts on water treatment plants (WTPs) and wastewater treatment plants (WWTPs) [1]–[18]. Tsunami, floods, and prolonged power outages are the indirect effects of the earthquake on treatment facilities. Direct effects include deformation and fractures in structural elements (e.g., pipes, tank walls, pool screens, bearing components), various damages due to ground liquefaction (e.g., settlements, collapses, slope flow), and damage to non-structural elements (e.g., scrapers, mixers, aerators, separator panels and curtains, monitoring, and control equipment) [19]. The effects that may cause damage can be examined under three main headings; (1) strong ground motion, (2) soil failure, (3) inertial forces [14]. Inertial forces cause sloshing in treatment tanks, depending on the geometry and depth of the unit and the earthquake characteristics. In addition to the damage of non-structural elements caused by the displacement due to fault rupture on the lithosphere, the sloshing in the tanks can also cause damage to the non-structural elements [6], [10], [12], [14], [17], [20]–[22].

The sloshing problem is a comprehensive phenomenon that has been studied for a long time in fields such as maritime, aviation, space technology, construction, geology, machinery, transportation, fuel storage, chemistry with the help of experiments and numerical methods. Field investigations after major earthquakes revealed that non-structural element damage due to sloshing in treatment plant units frequently occurred in the primary and secondary clarifiers and floating type oil removers [12], [14], [19], [23]–[25]. Rectangular type clarifiers are generally designed with 15 – 40 m streamwise length (L), length/width ratio (L/W) of 3 – 5, and 3 – 4.5 m average water depth (D) due to environmental engineering process optimization [26], [27]. Liquid sloshing investigations are based on detecting natural frequencies/sloshing modes, sloshing wave height, hydrodynamic pressure distribution, forces, and damping methods to suppress sloshing.

The sloshing wave height in a rectangular tank is the vertical displacement of the liquid surface caused by an external disturbance, such as a change in the tank's orientation or the introduction of a fluid into the tank. The natural frequency of the tank is the frequency at which the tank will naturally oscillate if disturbed. The natural frequency of a rectangular tank is dependent on the tank's dimensions and the fluid's density and can be calculated using the eigenvalue equation for the system. The sloshing wave height can be determined experimentally by measuring the displacement of the liquid surface, or it can be calculated using numerical simulations or analytical models[28], [29].

During the sloshing phenomenon, energy dissipation occurs because of viscosity, boundary layer development induced vortices near the wall, viscous boundary layers due to air-liquid interaction [30]. This dissipation brings out a damping effect to absorb liquid sloshing. Ibrahim [30] summarized that the damping factor is controlled by the liquid depth, the kinematic viscosity of the liquid, and tank diameter or tank width for a rectangular cross-section. At excitation periods close to the first natural period for fluid motion in the tank, even small motion amplitudes result in violent sloshing. A motion of the tank normal to the undisturbed free surface may excite symmetric modes, but since the maximum sloshing period is of primary relevance, vertical tank excitation is of secondary significance. First mode natural sloshing period of a rectangular tank is controlled via tank length and the filling depth [31]. For a low filling water depth (i.e., ($h/L < 0.2$) shallow water sloshing), wave run-

up occurs sidewall of the tank when the excitation period differs from the initial natural period of the fluid in tank. The angle between the free surface and the wall is modest, and the upward velocity of the water at their contact is high. Period of the motion effects the sloshing wave height and wave height inside the tank increases with the motion of the movement [32].

To decrease the sloshing-induced destructive hydrodynamic forces on the structure and suppress the sloshing waves, the efficiency of various applications (e.g., ring and cruciform baffles, floating baffles, lids and mats, flexible baffles, surface roughness increasing methods) were investigated. Fixed type baffles alter the volume of the sloshing domain, cause vortex generating with their sharp edges, and block the bulk climbing of liquid over the side walls [33].

Sloshing in rectangular tanks can be examined as a two-dimensional fluid motion. This two-dimensional flow can be classified under two sloshing behavior types: (1) low liquid fill depth, and (2) high liquid fill depth. If the ratio of liquid depth to the cross-sectional width of the tank in the direction of motion ratio is higher than 0.2, this case is classified as 'high liquid fill depth' [30]. If the aforementioned ratio is smaller than 0.2, typical for rectangular type clarifiers, the sloshing is classified as 'low liquid fill depth' (i.e., shallow water tank, or shallow type sloshing). In a shallow type of sloshing, hydraulic jumps and traveling waves for excitation periods around resonance were reported by various researchers [34]–[37]. This strong sloshing, accompanying waves and hydraulic jumps cause extremely high impact pressures on all kinds of structural (e.g., baffles, feeding wells) and non-structural elements (e.g., scrapers, chains, measurement probes) placed inside the tank or on the tank walls. Ibrahim [30] also pointed out that these impact pressures cannot be determined theoretically and need experimental and numerical work to be estimated. Non-structural elements inside WTPs and WWTPs units must be investigated under sloshing dynamics for a proper design. Aksel (2021) numerically modelled circular type of clarifier under earthquake-induced sloshing conditions, and pointed that non-structural element (i.e., feeding well) inside the units significantly affected the dynamic of the sloshing [38].

Damage to the treatment system will cause the treatment facilities, which will have a critical role in public health after the earthquake, to lose their functionality. WTPs and WWTPs that cannot continue their activities due to damaged facilities will prevent public access to clean water and healthy sewage treatment after the earthquake and impair public health. As seen in previous earthquake cases, this state of affair may cause epidemics and even loss of life [39]–[43].

Determining the fragility and sensitivity of the units in the treatment plants against potential earthquakes and taking necessary precautions are essential for protecting the environment and public health, and reducing the potential economic losses experienced afterwards. There are some estimation methods in the literature about determining the fragility of treatment plant units and the earthquake sensitivity of facilities [23], [44]–[47]. However, these methods do not clearly define/suggest limits for the design. Instead, they only allow risk estimation according to the soil condition of the facilities, the year of construction, the nature of the building material used, and the earthquake impact zone. Reducing possible risks before a potential earthquake is disproportionally more cost-effective and time-efficient compared to post-earthquake surveys of treatment facilities, repairing the detected damages, and re-commissioning the facilities [25], [48].

Based on the process optimization from an environmental engineering perspective, regulations, standards, and specifications prepared for treatment plants in the literature were regulated. These facilities, which are planned and designed without considering the dynamic building performance, are located in low-elevation and generally alluvial areas of the city most of the time, considering water collection convenience. This situation results with weak soil conditions, and it further increases the risk of damage to the facilities, which should be included in the critical facilities class with high earthquake risk [24], [44]. There is a lack of knowledge about the behavior of such facilities under earthquake conditions and their performance in the current earthquake regulations and standards, especially for earthquake-induced sloshing.

With this motivation, experimental and numerical studies were undertaken in this study. First, the response of a simplified rectangular type of water tank geometry under the influence of periodical motion was investigated experimentally. The experimental results were analyzed, and the generated data constituted a reference for the numerical model. Then, during the numerical model study, the same problem was reproduced in a numerical domain. The model's initial and boundary conditions were prescribed, and model parameters (e.g., roughness coefficient, mesh aspect ratio, interaction coefficient between phases) were defined accordingly. This step is followed by the validation of the model. After calibrating the numerical model concept, a widely used geometry was selected as a rectangular clarifier, and the vulnerable equipment (i.e., scrapers) was integrated into the model. The sloshing behavior was examined under two different earthquake signals (i.e., Chi Chi (1999), Kocaeli (1999)). The main goal of this study is to examine the effect of earthquake-induced sloshing on hydrodynamic stability of a commonly used rectangular type clarifier and hydrodynamic pressure variations on non-structural equipment (i.e., scrapers) during the sloshing.

2. MATERIALS AND METHODS

Examination of the damage on treatment plant units caused by sloshing, especially those of the vulnerable equipment inside them, using the full-scale studies requires a challenging and expensive research process. In line with this fact, in this study, a two-stage analysis was applied. Firstly, physical model studies were conducted. Then, this stage is followed by a numerical model study in which Reynolds-Averaged Navier-Stokes (RANS) equations were solved. During the computer-aided computation of sloshing in model tanks, model parameters, boundaries, and initial conditions were calibrated with the results of the experimental research.

Computational Fluid Dynamics (CFD) based sloshing analysis was performed using RANS equations with the help of Flow-3D software, which is commonly used in various disciplines [49]–[57]. CFD tools are used by various researchers for the design and operation of WTPs & WWTPs [58]–[62]. In addition, this solver has also been used in sloshing analyses with confirmation by experimental studies and calculates results compatible with the experimental results [63]–[65].

2.1. Model Validation

2.1.1. Experimental Setup

Experimental studies were carried out in the laboratory of the Civil Engineering Department of Alanya Aladdin Keykubat University. The testing system consists of a water tank with uniaxial freedom of movement, built on a monorail driven by a computer-controlled step motor, a shaking table. The water tank was 28 cm in length and 10 cm in width, and it was filled with 5 cm depth of red-colored water. An accelerometer capable of recording 100 Hz data that sends measurements to the computer was mounted on the shaking table. A video camera synchronized with accelerometer measurements was also used (Figure 1). To conduct the experiments under identical controlled conditions, room temperature and humidity were kept constant at 22 ^{o}C and 55%, respectively.

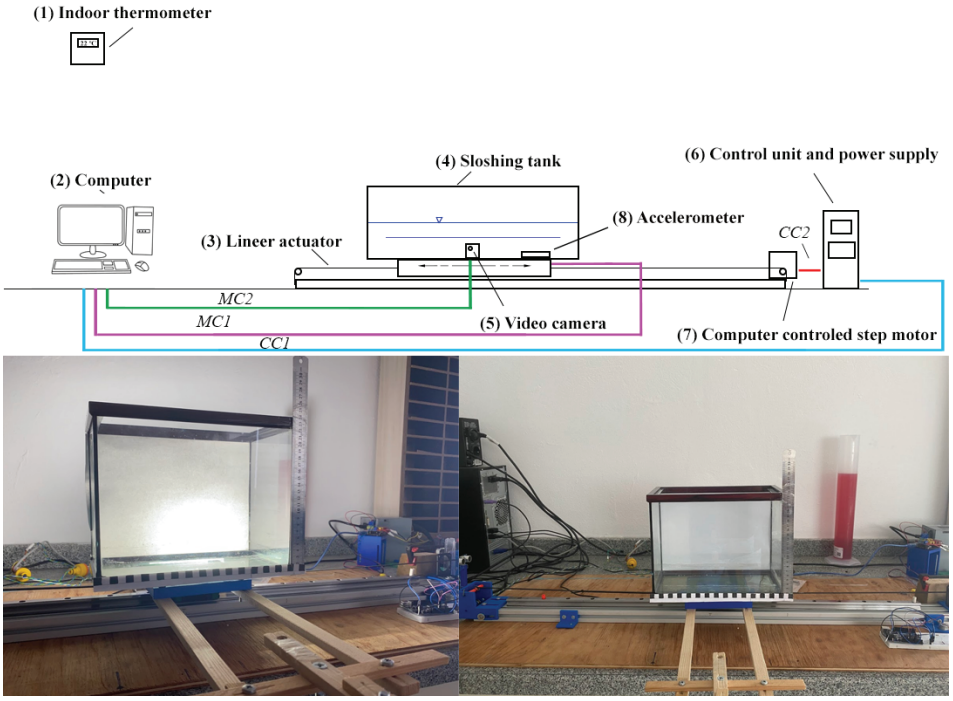

Figure 1 - Experimental setup (1) indoor thermometer, (2) computer, (3) linear actuator, (4) sloshing tank, (5) video camera, (6) control unit, (7) step type computer-controlled motor, (8) accelerometer. Green and red lines show control cables 1 and 2 (CC1), (CC2), and magenta and light blue colored lines present monitoring cables (MC1), (MC2), respectively.

In Figure 2a, the velocity vs. time signal used in the shake table and recorded velocity data from the accelerometer are presented with a dashed line and a solid red line, respectively. Input signal was sinusoidal, and the input signal period and amplitude were 2.81 sec and 4,62 m/sec, respectively. The incompatibility between the input signal and the speed data read on

the shake table stems from the errors originating from the entire system (e.g., measurement noise, motor response delay, belt system-induced oscillation). Nevertheless, the general behavior of the shaking table reflects the intended input signal. The main period of the tank motion, which is defined as the time for the moving tank to complete one full cycle in lateral direction (T_{ip}), was calculated via time differences between the successive local extrema in Figure 2a as 2.81 sec. In Figure 2b zero-crossing points for down/up are marked up the output signal. Mean period of the tank motion were calculated via MATLAB with an interpolation code for zero-up-crossing and zero-down-crossing as 2.76 sec and 2.68 sec, respectively.

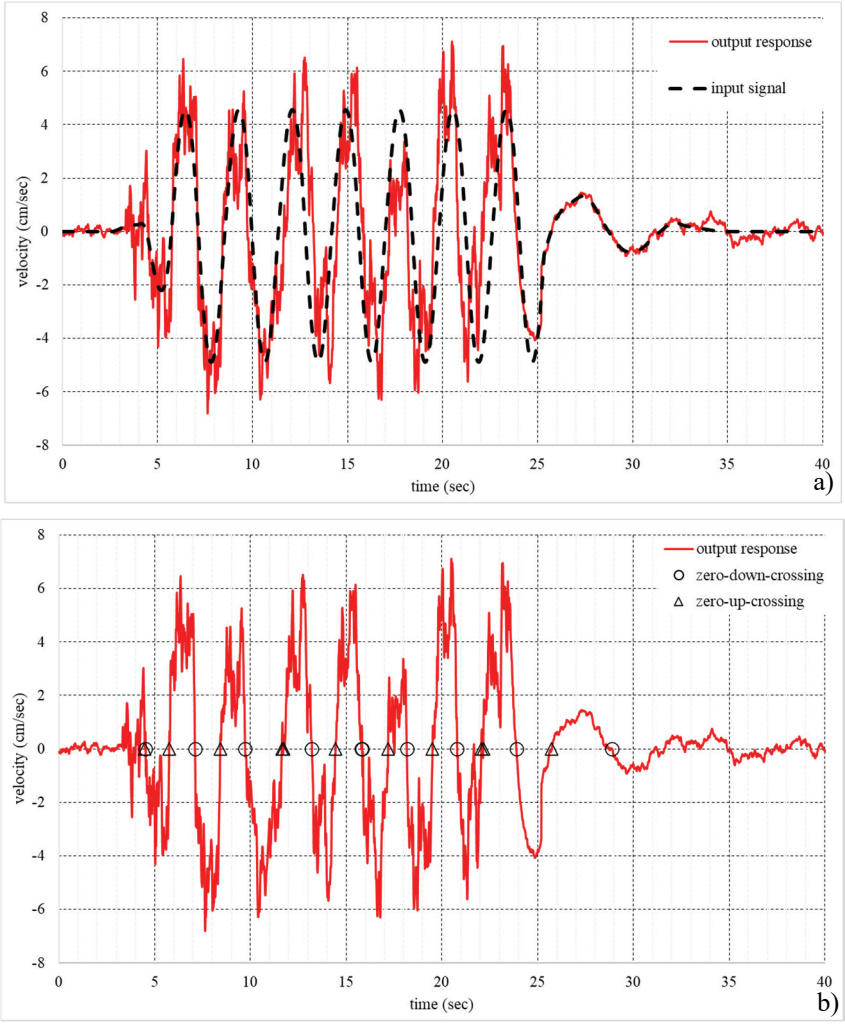

Figure 2 - a) Input velocity signal from the computer control unit (black dashed line) and recording from the accelerometer mounted on the shake-table (red line), b) output signal and zero down crossing (O)and zero down crossing (Δ) points

2.1.2. CFD Analysis for Validation

The basic equations of mass continuity and momentum balance was used in the numeric analysis, which are explained below.

$$V_F \frac{\partial \rho}{\partial t} + \frac{\partial}{\partial x}(\rho u A_x) + R\frac{\partial}{\partial y}\left(\rho v A_y\right) + \frac{\partial}{\partial z}(\rho w A_z) + \xi \frac{\rho u A_x}{x} = R_{DIF} + R_{SOR} \quad (1)$$

In Eq. 1, V_F is the fractional volume open to flow (i.e., flow domain), u, v, and w are velocity components, R is coordinate system conversion coefficient, ρ is the fluid density, ξ is the coordinate conversion parameter (ξ = 0 corresponds to cartesian geometry, while ξ = 1 corresponds to cylindrical geometry), R_{DIF} is a turbulent diffusion term, and R_{SOR} is a mass source term [66].

$$\frac{\partial u}{\partial t} + \frac{1}{V_F}\left\{uA_x\frac{\partial u}{\partial x} + RvA_y\frac{\partial u}{\partial y} + wA_z\frac{\partial u}{\partial z}\right\} - \xi\frac{A_y v^2}{xV_F} = -\frac{1}{\rho}\frac{\partial p}{\partial x} + G_x + f_x - b_x - \frac{R_{SOR}}{\rho V_F}(u - u_w - \delta u_s)$$

$$\frac{\partial v}{\partial t} + \frac{1}{V_F}\left\{uA_x\frac{\partial v}{\partial x} + RvA_y\frac{\partial v}{\partial y} + wA_z\frac{\partial v}{\partial z}\right\} + \xi\frac{A_y uv}{xV_F} = -\frac{1}{\rho}\left(R\frac{\partial p}{\partial y}\right) + G_y + f_y - b_y - \frac{R_{SOR}}{\rho V_F}(v - v_w - \delta v_s) \quad (2)$$

$$\frac{\partial w}{\partial t} + \frac{1}{V_F}\left\{uA_x\frac{\partial w}{\partial x} + RvA_y\frac{\partial w}{\partial y} + wA_z\frac{\partial w}{\partial z}\right\} = -\frac{1}{\rho}\frac{\partial p}{\partial z} + G_z + f_z - b_z - \frac{R_{SOR}}{\rho V_F}(w - w_w - \delta w_s)$$

Here, in Eq. 2, G_x, G_y, G_z are body force components, A_x, A_y, A_z are the directional open area to flow, f is viscous force, b is flow losses in porous media/across porous baffle plates, and the final terms account for the injection of mass at a source represented by a geometry component. U_w (u_w, v_w, ω_w) is the velocity of the source component, U_S (u_S, v_S, ω_S) is the velocity of the fluid at the surface of the source relative to the source itself, and δ = 0.0 in Eq. 2 the source is of the stagnation pressure type. If δ = 1.0, the source is of the static pressure type. Thus, it is possible to define a linear acceleration or direction-based velocity using moving object physics in Flow-3D. The general moving object (GMO) mechanism that is either user-specified (prescribed motion) or dynamically connected with fluid flow (coupled motion). The motion of a rigid body can typically be described with six velocity components: three for translation and three for rotation. To accurately interpret the computational results and define the motion of a GMO, a user must comprehend the body-fixed reference system (body system), which is always fixed on the object and experiences the same motion [66].

Volume fraction change with time in Eq. 1 is replaced by $\vec{V}_{obj}.\vec{n}\,S_{obj}/V_{cell}$ for defining the mass conversation property of fluid, where S_{obj}, $\vec{n}$, and $\vec{V}_{obj}$ are surface area, surface normal direction and velocity of moving object boundary in a mesh cell, respectively [67].

The accelerometer record presented in Figure 2 was directly used to describe tank motion in the CFD verification analysis.

The fluid domain was divided into a quadratic type of mesh elements for calculations. Side and bottom walls were defined as wall type boundaries with no-slip conditions, and the top boundary was selected as relative pressure type boundary, which is equal to zero relative pressure magnitude. This boundary allows two-way fluid mass inlet-outlet, however in the model no water phase was defined nearby, it was set as stationary air phase. Compressibility was neglected for the fluids (both air and water) in model. Renormalized group (RNG) type of turbulent model was employed for turbulence closure. The water depth was set to 0.05 m, and physical water properties (e.g., density and viscosity of water, water-air interface entrainment, these parameters were taken as 22°C water temperature characteristics) were arranged identical with the experimental conditions. The water depth was selected to facilitate shallow water sloshing. The standards published by the American Society of Mechanical Engineers (ASME, 2009) were followed during the validation of the CFD model [68].

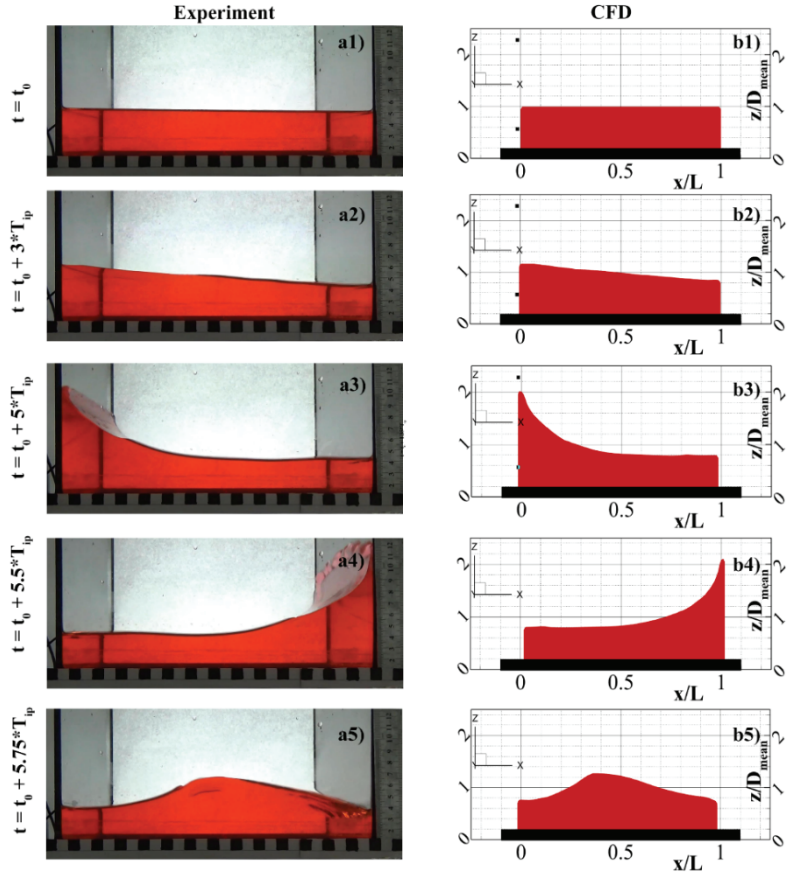

Figure 3 - Visual verification of the model outputs a1-a5) the pictures captured from the video and b1-b5) CFD model results for the water phase. The dimension of the ruler adjacent to sub-figures "a" is in cm. The squares located at the bottom of each sub-figures "a" are 1 cm x 1cm.

Images captured during the physical model tests of sloshing and CFD model results in the corresponding moment are given as couples in Figure 3. In addition, temporal information on which moment the results belong is presented on each figure's left side. Here, t is the instantaneous time, and t_0 is the initial time for both experimental and CFD analysis. The tank's sloshing period (T_{ip}) was calculated as 0.8 sec using Eq. 3 [69], in which L is the length of the tank in motion direction, g is gravitational acceleration, and D_{mean} is the depth of the fluid at rest inside the tank.

$$T_{ip} = 2\,\frac{L}{\sqrt{g.D_{mean}}} \tag{3}$$

Visual comparison of the presented images belonging to the experiment and numerical model showed that the numerical model can simulate the sloshing process in the tank with acceptable accuracy. For a detailed quantitative analysis image processing tools were utilized to detect the left side wave height (i.e., instantaneous water level at the left edge of the tank) during the sloshing. Frames were exported from the video captured with a 60-fps rate. Firstly, masking was utilized to detect only red pixels. Secondly, the masked image was converted into a black-white image. Edge detection and corner detecting were applied on the frames to calculate the y coordinate of the top-left edge of the white-colored fluid domain (Figure 4). After all, pixels were counted automatically, and pixel coordinate was converted to water depth values. On the other hand, a probe was placed at the left side of the tank in the CFD model to calculate water depth during the analysis. The timeseries of water depth values from the image processing of experimental results and those from the CFD analysis are presented in Figure 5. As seen, a fair agreement between the experimental and numerical results is evident. In Figure 5b, relative errors of CFD results for minima and maxima extreme values due to image process results were given using bar and triangle, respectively. Extreme values (i.e., minima and maxima) were calculated using MATLAB signal processing tools for first 35 sec after the initial motion. This experimental setup and validation procedure were also used to model spherical particle behavior under sloshing event [70].

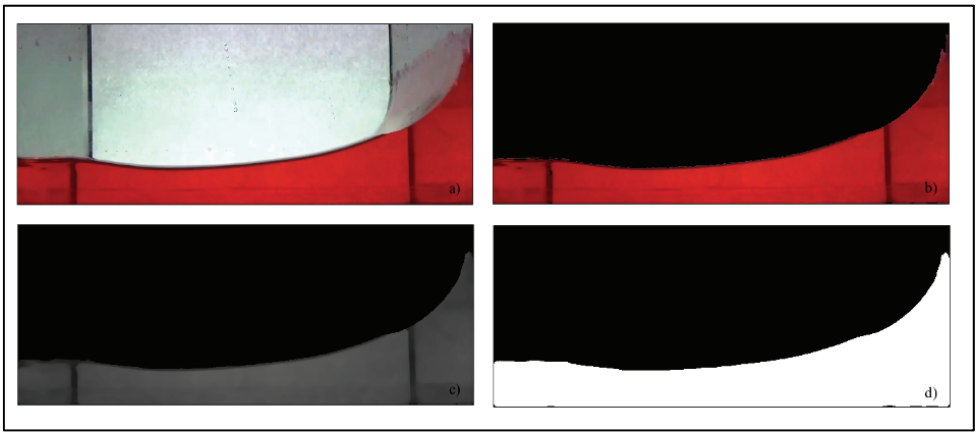

Figure 4 - Image processing procedure a) importing raw image, b) masking un-red pixels, c) converting grayscale and denoising, and d) converting black& white.

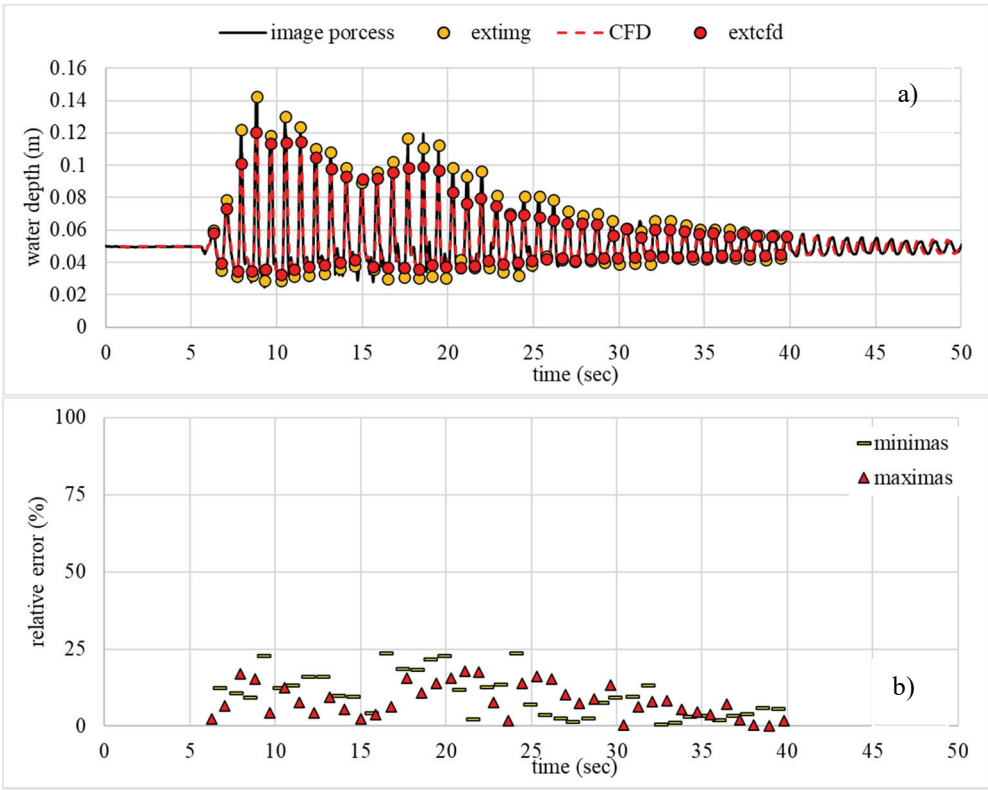

Figure 5 - a) Water depth at the left-hand side of the tank during the test 1 was calculated via image process and CFD. Image process and CFD results were presented with black and red lines, respectively. Yellow and red dots show minimum and maximum extremes for image process and CFD results, correspondingly. b) Relative errors of CFD results for minima and maxima extreme values due to image process results were given using bar and triangle, respectively.

2.2. CFD Model Analysis for Rectangular Type Clarifier

Rectangular type clarifiers include various pieces of equipment inside for process, sedimentation, and flow control (i.e., inlet baffles, flights, weirs, drive chains or belts, rails, monitoring probes, water, and sludge level sensors, scum collectors). This equipment is sensitive and vulnerable to hydrodynamic impacts. In the following sub-sections, first, the geometry of the operating conditions simulated by the numerical model is identified. Second, an earthquake-induced sloshing model is defined which was run using historical earthquake signal datasets.

Mesh and model characteristics are summarized in Table 1 for CFD models. Mesh quality effect on sloshing behavior calculation was performed by Gandara et. al. (2021) with an 800 mm tank and various mesh size. In their study, experimental tank volume / mesh number ratios were taken between $0.79 \times 10^{-6} - 2.26 \times 10^{-6}$ m^3/element. Improved mesh

quality (0.79×10^{-6} m^3/element ratio) was sufficient to represent the sloshing behavior inside a rectangular tank [71]. During the modelling calculations in scope of this work experimental tank volume / mesh number ratio was employed as 1.56×10^{-8} m^3/element.

Table 1 - Mesh and Model Characteristics

	Validation Model	**Real Scale Clarifier Model**
Mesh Type	Uniform Quadratic	Uniform Quadratic
Mesh Size (m)	0.0025	0.01
Number of Mesh	1002240	11648000
Dimension	3D	3D

2.2.1. Geometry Selection and Operating Conditions

To examine the earthquake-induced hydrodynamic pressure values acting on vulnerable equipment inside a rectangular clarifier, firstly, a characteristic tank geometry representing the average dimensions due to the standards was prepared. According to the average values of the ranges given by Metcalf & Eddy (2003), the prototype clarifier dimensions were chosen as L=30 m, W=6 m, and D_{mean} = 4 m. The sloshing period (T_P) for the selected clarifier dimensions was calculated as 9.58 s using Eq. 3. The average operation flow rate was taken as 0.125 m^3/s to satisfy the typical value of overflow rate, which is approximately 60 m^3/m^2 /day [27]. Water was assumed as clear water (i.e., no sludge inside the tank), and the temperature was chosen as 20 °C to configure physical parameters belonging to water.

A perspective view of the model domain with essential equipment inside and layout of numerical probes (shown as red dots) included in the model is presented in Figure 6. Still water level (SWL) was selected as 4.35 m from the tank bottom. The inlet boundary was pointed on the left-hand side, and the outlet weir was marked on the right side. The probes labeled as 1 and 2 are located in the front and back of the velocity reducing (pressure break) panel. Probes 3 and 4 are installed in front and behind of the outlet weir, respectively. The labeling of the monitoring probes for scrapers was based on the direction of the flow; the ones starting with the "u" code represent the near-surface location (z = 4.3 m), and the ones beginning with the "d" code represent the near-bottom (z = 0.8 m) points. The number sequence is given in the streamwise direction. Odd numbers indicate the upstream side of the obstacles, and even numbers indicate the downstream probes. The probes are shown as red dots in Figure 6.

The model representing operating conditions was run until the model's mass average kinetic energy value became stable. It took 6000 s (in the model time) to reach the steady-state conditions in the model environment. This value corresponds to four computer calculation days. When the model output stabilized, the earthquake analyses were initialized with the numerical model, using the steady-state operating conditions as an initial condition. In Figure 7, the flow pattern is plotted at the longitudinal centerline of the clarifier for stable (steady state) operating conditions. As seen in Figures 7a and 7b, representing t=3000 s and t=6000 s, respectively, the model became stable.

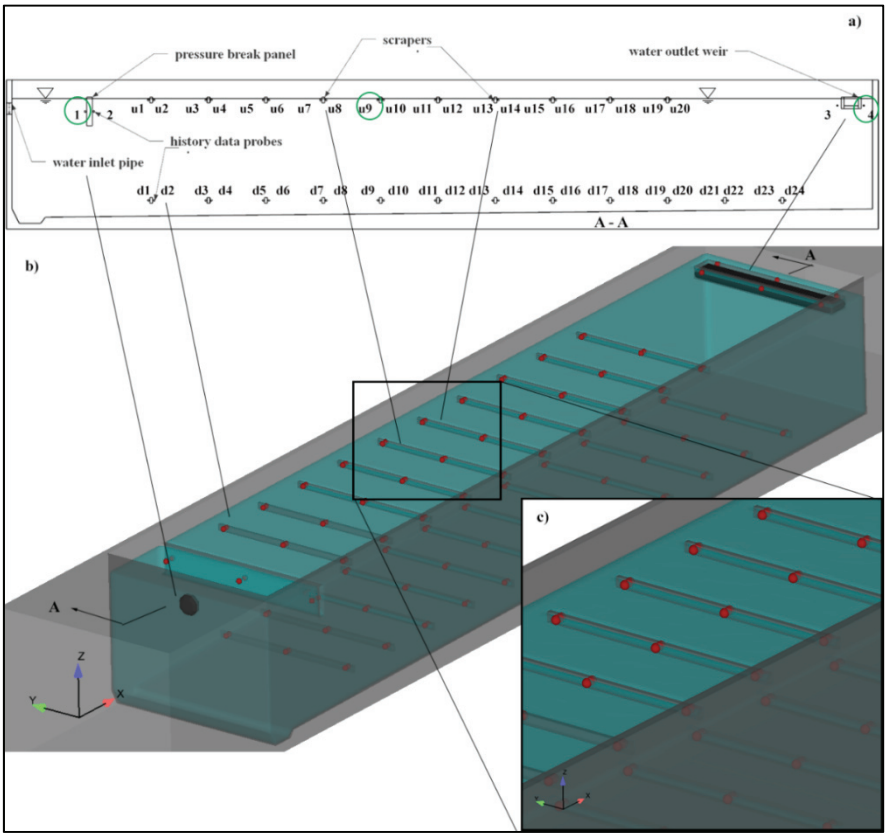

Figure 6 - The centerline of the longitudinal cross-section of the model includes fundamental elements and calculation probes. The red dots in subfigures b and c indicate the numerical probes. In subplot a, the green circles correspond to the locations where the analyses were carried out/presented in Fig 7.

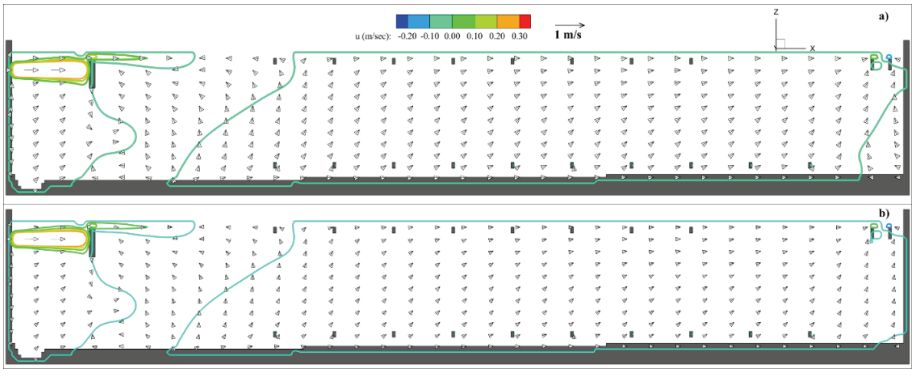

Figure 7 - Flow pattern inside clarifier under operating conditions a) t = 3000 s, b) t = 6000 s.

2.2.2. Earthquake Induced Sloshing Model

The general moving object model which is a rigid body with any kind of motion that is either user-prescribed or dynamically coupled with the fluid flow was selected to simulate clarifier response to the seismic motion. The hydrodynamic response of the rectangular type of clarifier under the earthquake-induced sloshing effect was investigated by accepting the model that has stabilized under the operating conditions as the initial condition. The clarifier was assumed to be a rigid moving element with equipment inside and would move simultaneously with the ground motion. The ground motion time series was created using velocity-time data from two well-known earthquakes, i.e., Chi Chi (1999) and Kocaeli (1999). Earthquake signals were downloaded from the Pacific Earthquake Engineering Research Center (PEER) Ground Motion Databases (PGMD).

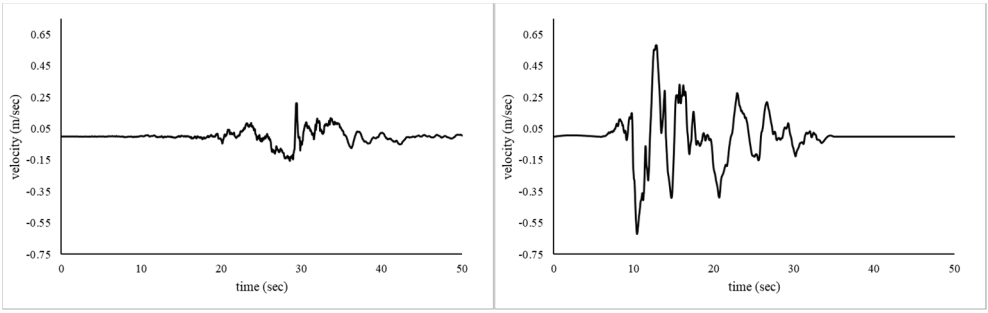

Figure 8 - Ground motion signals of a) Chi Chi (1999) and b) Kocaeli (1999) earthquakes.

In Figure 8, the time series of the ground motion velocities for Chi Chi (Figure 8a) and Kocaeli earthquakes (Figure 8b) were used directly (without any denoising or smoothing operation) in the model to define the prescribed one-directional motion to the clarifier. Although both Chi Chi and Kocaeli earthquakes have close maximum peak acceleration values (0.361 and 0.349 g, respectively), the specific energy density of the Kocaeli earthquake (1.0334 m^2/s) is approximately 12 times higher than that of the Chi Chi earthquake (0.08812 m^2/sec) (PEER-PGMD). During the earthquake-induced sloshing simulations, the operational flow rate input was stopped for the sake of simplification in the model, assuming a power outage during the earthquake.

3. ANALYSIS OF THE RESULTS

As stated above, the steady flow conditions were used as the initial condition. Then on top of the steady flow conditions, two different earthquake characteristics were applied. The hydrodynamic response of the clarifier was investigated under these two characteristic cases. The clarifier's center is represented by point u11, which was nearly located at the center of the scraper group (Figure 6). On the right-hand side, in the streamwise direction, point 4 was located near the outlet weir. Point 1 was located at the front side of the pressure break weir near the inflow.

In Figure 9, the temporal variations of water surface fluctuations at these three locations (i.e., points 1, u11, 4) under the effect of two characteristic earthquakes (i.e., Chi Chi and Kocaeli) are given. As seen from Figure 9, the sloshed wave heights, which are presented for points 1 and 4, were higher than the center point (i.e., u11). This result implies that the hydrodynamic forces acting on the clarifier at both edges are more critical than at the center zone, as also observed in the experiments. Second, the magnitude of extreme waves in Figure 9 is proportional to time variation of earthquake acceleration. Since the specific energy density belonging to Kocaeli earthquake is higher than the one in Chi Chi (Figure 8), the developed extreme sloshing waves do not attenuate rapidly, and the wave damping process takes markedly longer in the former case.

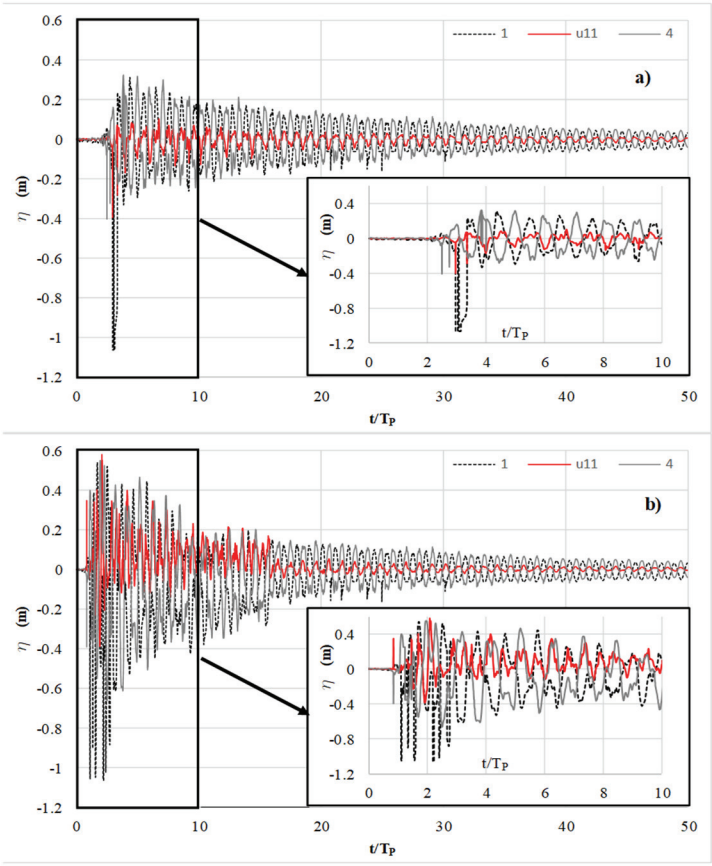

Figure 9 - Water surface displacement under a) Chi Chi earthquake b) Kocaeli earthquake for monitoring points left side (1 – dashed line), center (u11 – red line), and right side (4 – grey line) of the clarifier on cross sectional view. Points are marked with green circle on Fig. 6. The insets show the time-intervals where the analyses were given in Fig. 10 and 11.

In Figure 10, water surface displacement values which were presented in Figure 9a and b for Chi Chi and Kocaeli were analyzed using MATLAB signal processing tools and were plotted in frequency domain. Fast Fourier Transformation (FFT) was applied during this conversion. Natural frequencies for the first ten modes of the rectangular clarifier were calculated and marked up Figure 10 with blue circles.

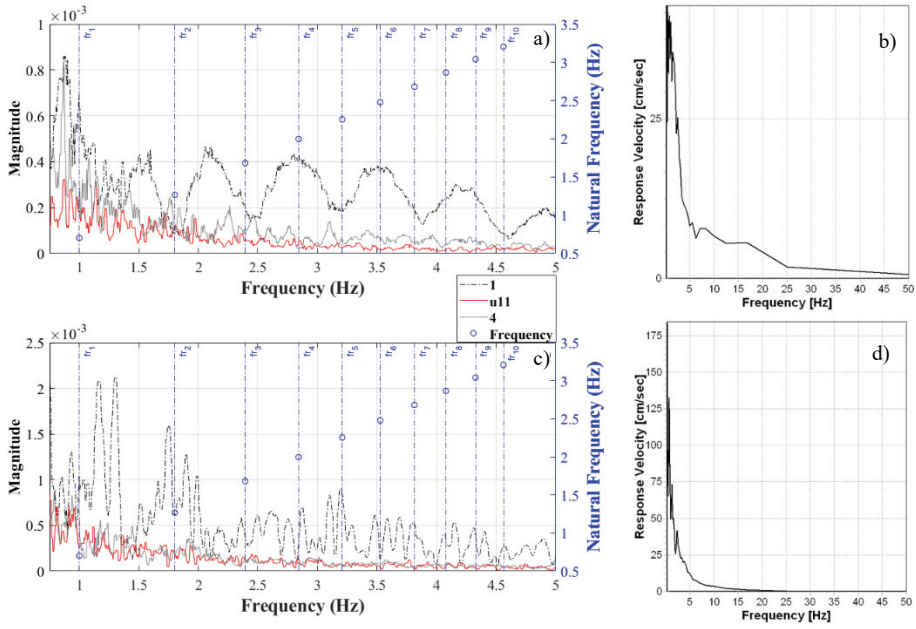

Figure 10 - Sloshing wave height magnitude in frequency domain a) Chi Chi earthquake c) Kocaeli earthquake for monitoring points left side (1 – dashed line), center (u11 – red line), and right side (4 – grey line) of the clarifier on cross sectional view. Points are marked with green circle on Fig. 6. Blue marks are the natural frequencies for the first 10 modes of the clarifier. Earthquake response velocities are in frequency domain for b) Chi Chi and d) Kocaeli.

In Figures 11 and 12, clarifier responses to Chi Chi and Kocaeli earthquakes are presented for the selected time intervals. On these charts, the normalized pressure distributions (P/P_∞) were denoted by solid pink circles. Normalization was carried out based on the pressure value (P), which arises during the normal operation of the system (P_∞), i.e., before the earthquake starts. It is evident from Figure 11 that for the case of Chi Chi earthquake, the individual instantaneous extreme pressure values were observed at the right and left-hand sides of the pressure break weir. In Kocaeli case, the instantaneous extreme pressure values in Figure 12 similarly concentrated around the pressure break weir. However, it is also worth mentioning that since the specific energy density of Kocaeli earthquake is significantly higher compared to Chi Chi, the same situation was observed in a more pronounced manner for this case.

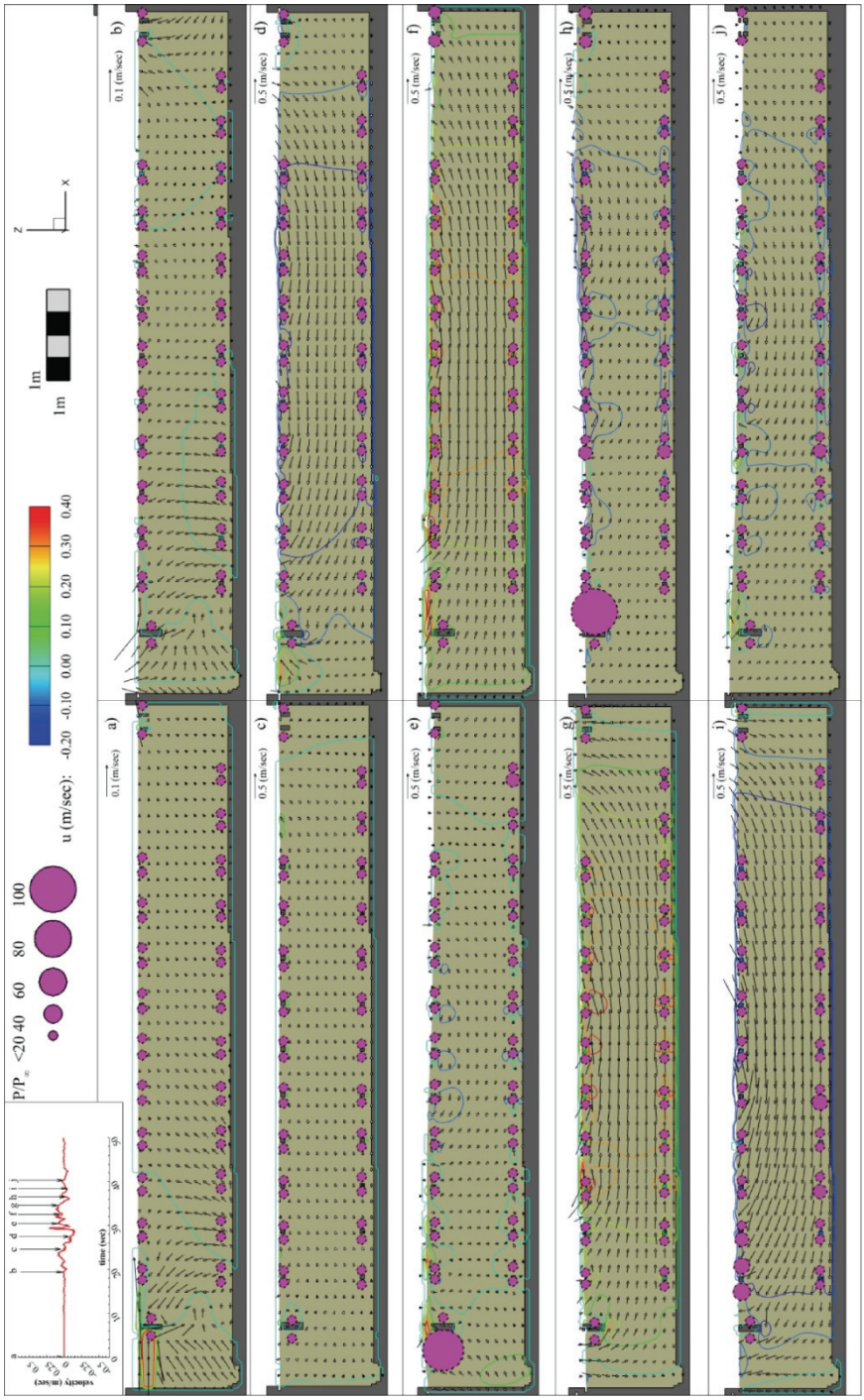

Figure 11 - Clarifier response to Chi Chi earthquake for selected time a) t_0, b) $t_0 + 2*T_P$, c) $t_0 + 2.5*T_P$, d) $t_0 + 3*T_P$, e) $t_0 + 3.2*T_P$, f) $t_0 + 3.4*T_P$, g) $t_0 + 3.6*T_P$, h) $t_0 + 3.8*T_P$, i) $t_0 + 4*T_P$, and j) $t_0 + 4.2*T_P$

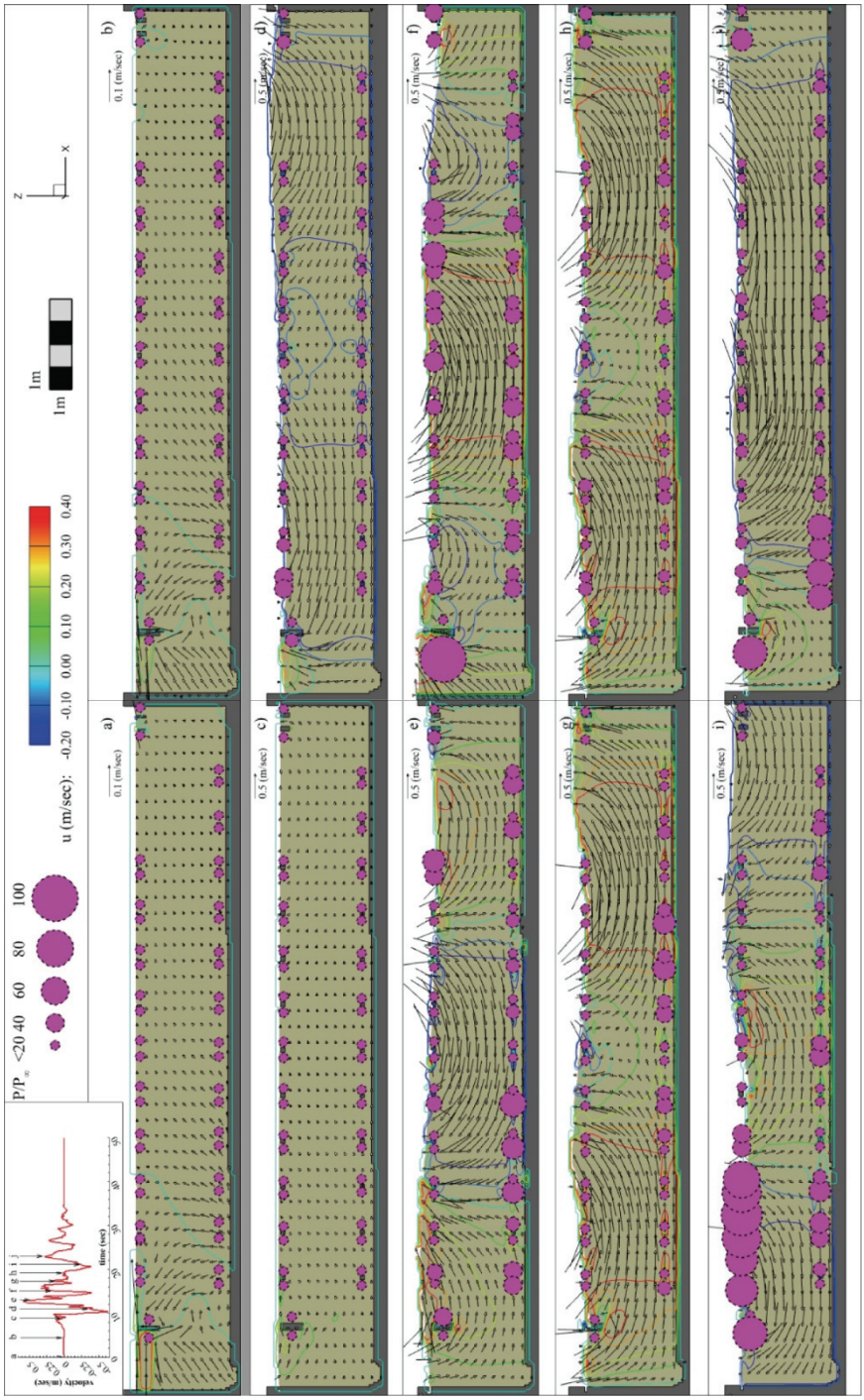

Figure 12 - Clarifier response to Kocaeli earthquake for selected time a) t_0, b) $t_0 + 0.5*T_P$, c) $t_0 + T_P$, d) $t_0 + 1.2*T_P$, e) $t_0 + 1.4*T_P$, f) $t_0 + 1.6*T_P$, g) $t_0 + 1.8*T_P$, h) $t_0 + 2*T_P$, i) $t_0 + 2.2*T_P$, and j) $t_0 + 2.4*T_P$

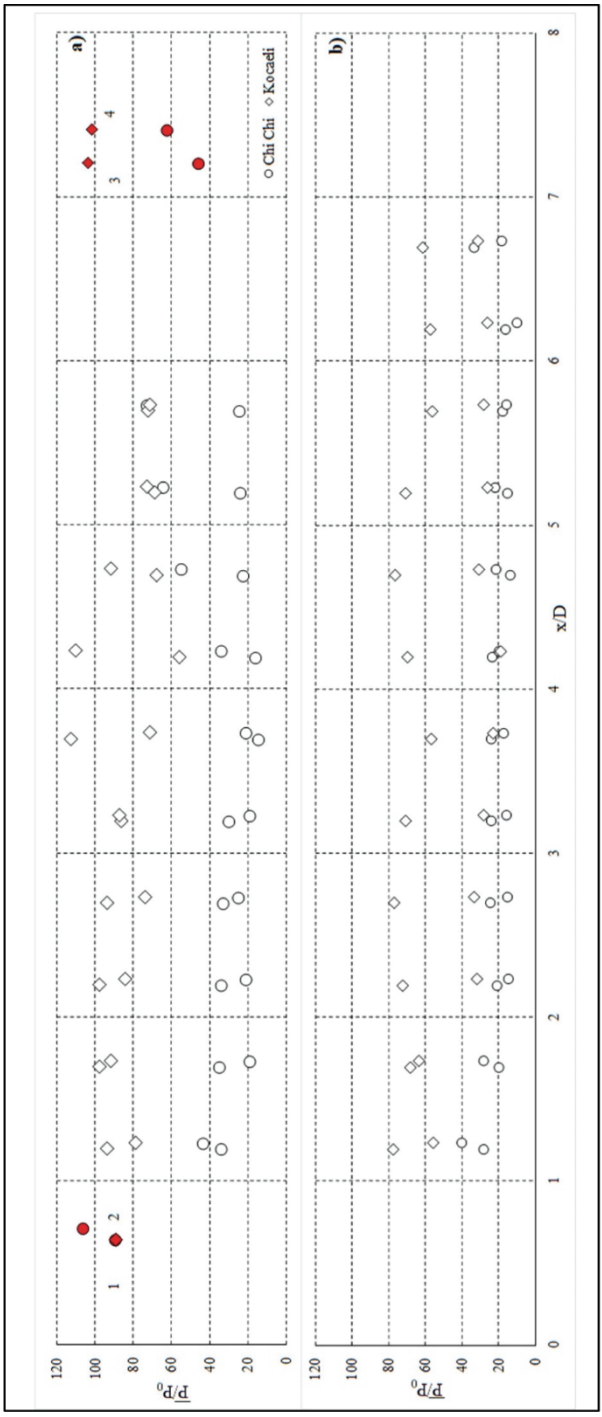

Figure 13 - Observed normalized maximum dynamic pressures at a) monitoring points near water surface (z=4.3 m) b) near bottom monitoring points (z=0.8 m). Red dots are named monitoring points belonging to inlet and outlet panel/weir. Diamonds and circles represent results of Kocaeli and Chi Chi earthquakes, respectively.

The instantaneous high-pressure values around scrappers are distributed unevenly under the sloshing condition of Kocaeli earthquake, differing from Chi Chi earthquake. When the relationship between velocity vectors and the emergence of extreme pressure zones are evaluated, it can be concluded that the extreme pressure values arise when two coherent flow domains converge to and diverge from each other.

In Figure 13, the average of maximum three normalized pressure values ($\bar{P}/P_0$) observed, occurring around each component (i.e., scraper and weirs), are presented; $\bar{P}$ is the time-averaged pressure value and P_0 is the hydrostatic pressure at calculation point. In line with Figures 11 and 12, the pressure values are quite high in the vicinity of the weirs. Besides, other extremes, which were not captured in flow domain analysis given for consecutive time steps (in Figures 11 and 12, only visualization was made for a certain time interval) presented in Figures 11 and 12, were calculated exactly at the center of the clarifier.

4. DISCUSSION AND RECOMMENDATION

Sloshing is a non-negligible governing factor in the design of wastewater treatment plants and the treatment capacity and efficiency, especially in high earthquake risk zones. Necessary measures should be taken to prevent/diminish any potential damages of equipment, which are vulnerable to earthquake-induced sloshing, inside the clarifiers. Limit situations should be determined considering earthquake-induced sloshing effects, and the standards should be formed according to these limit situations (e.g., freeboard, risk of damage for the sensitive equipment). This study was conducted to highlight the significance of the sloshing in clarifier. It was also aimed to present a fundamental knowledge which may aid in design of rectangular type clarifiers under earthquake conditions. The assumptions made in the model approach (RANS as turbulence model, surface tension, surface roughness) and mesh quality cause the model to calculate underestimated wave heights than the experiment, especially at peak values. In addition, the analysis of the test results with the image processing technique causes the splashes that occur during agitation to be detected as a continuous fluid phase. This causes a 13% relative error in the peak value at the 10^{th} second of the analysis.

Previous studies on sloshing show that there is a relationship between natural frequency and sloshing wave. A similar relationship is also observed in this study as depicted in Figure 10. However, an important finding is that there is a delay caused by scrapers in the relationship between the sloshing and the natural frequencywhich becomes more evident as the earthquake intensity increases so that the correlation between the natural frequency and the sloshing wave decreases (Figure 10b. Kocaeli). This relationship reflects the facts that the natural frequency of the clarifier is related to the properties of the fluid and the tank and the sloshing wave height is related to the amplitude of the liquid surface displacement caused by an external excitation. However, the presence of scrapers in the tank can introduce a delay in between natural frequency and the sloshing frequency, particularly as the intensity of the disturbance (such as an earthquake) increases. The scrapers can cause additional damping in the system, which can affect the natural frequency and the sloshing wave height.

The effect of compressibility, adhesion interaction with wall surfaces, cohesion and air entertainment were neglected during the calculations. These parameters have effects on the sloshing behavior and on the model results. Air compressibility can affect the amount of air entrapped in the liquid, which can change the overall weight and volume of the liquid. Water

compressibility, on the other hand, can change the density of the liquid and affect the pressure on the container walls. These factors can affect the amplitude and frequency of the sloshing motion, as well as the stability of the liquid.

Adhesion and cohesion forces can affect the behavior of the liquid in several ways:

- Adhesion forces can increase the amplitude of the sloshing motion by creating a sticking effect between the liquid and the container walls. This can cause the liquid to cling to the walls and move with them, leading to larger sloshing motions. For the future studies it is recommended to examine this phenomenon more closely.
- Cohesion forces can decrease the amplitude of the sloshing motion by creating a resistance to motion within the liquid. This can bring about enhancement in temporal lag between tank motion and wave. However, further effort is needed to investigate this aspect of the phenomenon.

The effect of the neglecting adhesion can be clearly seen, especially in the differences between the results of image processing and CFD analysis. In video images the splashes and the water droplets could be identify as water domain during the calculations. Additionally, lack of air entrainment during the modelling was affected the phase changing, air entrapping and variation in fluid density.

During sloshing, the hydrodynamic pressure at the bottom of a tank can vary greatly depending on the amplitude and frequency of the sloshing motion. The pressure can fluctuate significantly as the fluid in the tank moves back and forth. The highest pressure occurs at the location of the bottom of the tank when the fluid surface is at its highest point. The pressure can also vary depending on the properties of the fluid, and the geometry of the tank. In addition, the frequency of the sloshing motion and the amplitude of the sloshing can also greatly affect the pressure distribution inside the calculation domain. When all of these governing parameters (flow domain, fluid properties, and sloshing characteristics) are adequately reproduced in the model domain, the resulting pressure values will always be within an acceptable error of the actual values. Image processing techniques are used here to capture sloshing wave height and fluid motion, as well as to investigate sloshing dynamics in the literature. In order to perform a more precise analysis and obtain accurate results, it is recommended that the scalar variables (e.g., pressure) and kinematic variables (e.g., velocity) must be measured with non-intrusive measurement devices in the future studies.

The primary objective of the experimental effort was to determine the capabilities of the turbulent model, initial and boundary conditions of the code. In the rectangular-type clarifier response under the seismic condition scenario, real-scale tank geometry was used, which was larger than the tank in the validation section. Geometric scale-up can have a significant effect on the results of a CFD model.

It is a standard practice to employ model tests to evaluate various types of tanks, while quantifying their efficiency in the field. 1/25 to 1/70 is the optimum scale for model testing [72]. Jeon et. al., (2008) disclosed that scales between 1/25 and 1/50 are reasonable scales in terms of keeping the governing forces reasonably proportional. Nevertheless, 1/100 can be regarded as too small [73]. Froude scaling is a commonly employed scaling law in a sloshing model test [72]–[74]. To compare the scaling effect in a more efficient manner, the CFD analysis of the experimental system was repeated by scaling up the model by a factor of 107

using Froude scaling (geometrical scale=1/107). The scaling was carried out according to the dimensions and time scale as stated in the sloshing model test procedure document [74]. The reason for choosing a scaling factor of 107 in Froude scaling is that the ratio of the length of the experimental tank (Lp=0.28 m) (and thus the validation model) to the tank length in the clarifier models (Lm=30 m) is Lm/Lp=107. Figure 14 presents the effect of scaling on the sloshing wave height (water depth at the left side of the tank) and pressure value in time. The values are compared for the point presented in Figure 5. Furthermore, maximum errors of 28% for wave height and 20% for pressure have been calculated. By conducting experimental studies in a larger tank environment and scaling up the experiments, these error rates can be further reduced.

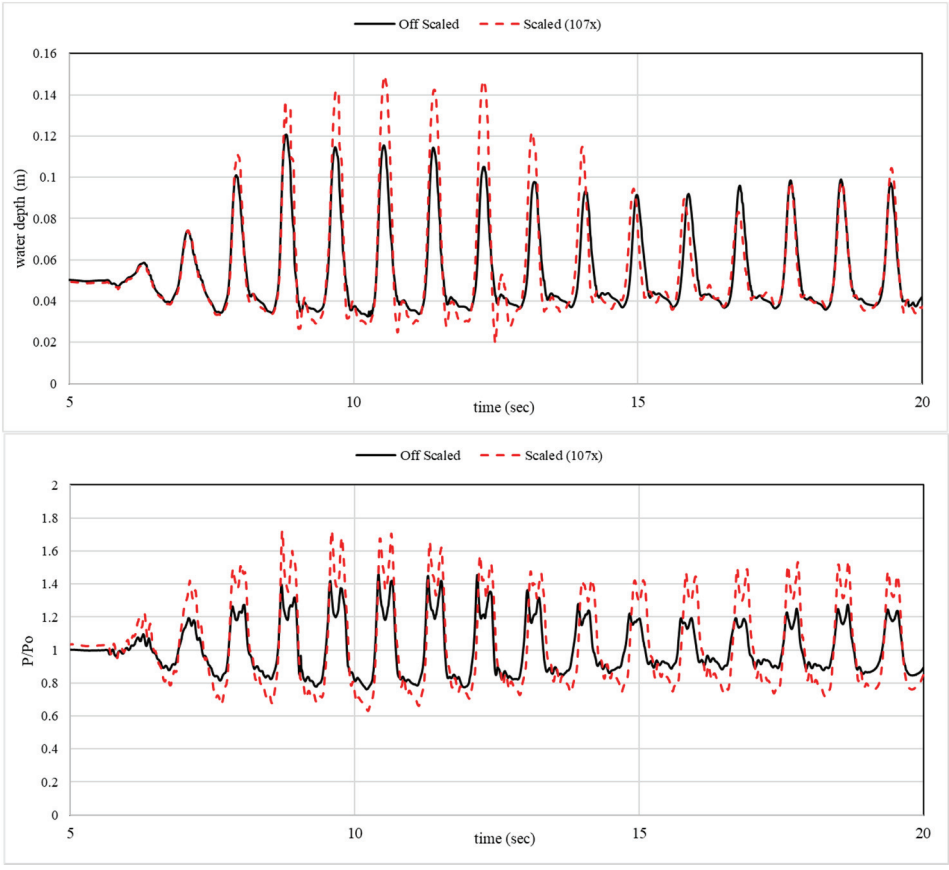

Figure 14 - Comparative graphics for off scaled (black solid line) and scaled (107x – red dashed line) a) water depth b) P/Po.

In this study, two historical earthquakes were considered as characteristic drivers to produce a sloshing effect in a typical clarifier. The characteristic earthquakes with similar periods were selected to make an efficient direct comparative analysis. It should be noted that the earthquake with various periods would results with different sloshing effects than the ones

presented here. The presented results should be evaluated within this perspective, as a realistic demonstration of the earthquake-induce sloshing process.

Sloshing waves are superimposed at the center of a clarifier. The resulting wave height and pressure can be affected by the amplitude, frequency, and phase difference of the individual waves (Figure 13). The superposition of waves can result in destructive interference, which can either amplify the total wave height and pressure at the units and causes failure of non-structural elements. The superposition of waves is a complex phenomenon, and it is influenced by many factors such as the properties of the fluid, the geometry of the tank, and the type of excitation (such as harmonic or random).

It is recommended that further parametric studies are performed to investigate the impact of the earthquake characteristics on the hydrodynamic pressures acting on the clarifiers. It is also suggested that the results of these parametric analyses are used to generate a set of non-dimensional empirical relationships between the earthquake parameters (such as the peak period, PGA, etc.) and the sloshing-induced loads on clarifier components. Besides, a characteristic clarifier with typical specific dimensions obtained from [27]was selected, and the modeling study was conducted for the clarifier with these dimensions. However, it should be noted that even under the identical period, different clarifier dimensions would lead to different loads on the equipment in the clarifier. Hence, it is recommended that the influence of clarifier dimensions on the emerging hydrodynamic loads under the sloshing effect are investigated.

5. CONCLUSION

In this study, a numerical model, which was validated against an experiment, was undertaken to simulate earthquake-induced sloshing in a clarifier. Once the model validation was accomplished, the following conclusions were drawn from the CFD analysis of a clarifier with typical full-scale dimensions, with which the hydrodynamic loads on equipment in the clarifier were analyzed under two historical earthquake signals.

1) From the spatial distribution of wave height within the clarifier obtained by the numerical model, it was seen that wave heights due to sloshing were higher near the edge sides of the tank compared to those in the center. This primary finding can be interpreted as the sloshing-induced forces acting on the clarifier and the equipment located at both edges being more severe than the center zone.

2) The simulations showed that the instantaneous extreme pressure values intensified around the pressure break weir. It was also seen that this situation becomes more pronounced as the enhanced specific energy density of the earthquake enhanced.

3) The findings revealed that the characteristics of the extreme waves (i.e., sloshing duration and wave heights) which were generated during the sloshing were well correlated with the time variation of earthquake accelerations. In other words, the higher waves generated under the high acceleration sloshes in the clarifier had relatively longer durations and damped significantly later. Once it is considered that the duration can be a significant factor in fatigue and causing damage to devices in the clarifier, the meaning of this finding is recognized better. This finding is in good harmony with the pertinent findings in the literature.

4) It was seen that under the influence of the sloshing, the extreme pressures are generated at the locations where two coherent flow domains with opposite flow directions meet each other within the clarifier.

5) The analysis of pressure domains indicated that the weirs are exposed to a higher-pressure effect compared to the scrapers. This finding shows that the weirs are more sensitive under the earthquake-induced sloshing event compared to other components. Hence, special attention should be given to these vulnerable units at the design stage for the clarifier. The results presented on pressure are based on the results of a numerical model that has only been validated against water level measurements and not some dynamic pressure measurements. As a result, these results contain some errors due to a variety of factors (numerical schemes, air entrapment, compressibility, etc.) and require additional investigation.

References

[1] EERI, "Earthquake of January 17, 1995: Reconnaissance Report," Oakland, California, USA, 1995.

[2] EERI, "The Nisqually Earthquake of 28 February 2001: Preliminary Reconnaissance Report," Oakland, California, USA, 2001.

[3] C. Strand and J. Masek, "Sumatra-Andaman Islands Earthquake and Tsunami of December 26, 2004 Lifeline Performance," Reston, VA, USA, 2007.

[4] R. Kayen *et al.*, "Investigation of the M6.6 Niigata-Chuetsu Oki, Japan, Earthquake of July 16, 2007, Report 2007-1365," 2007.

[5] A. K. Tang and A. Schiff, "Kashiwazaki, Japan, Earthquake of July 16, 2007, Lifeline Performance," Reston VA, USA, 2010.

[6] N. L. Evans and C. Mc Ghie, "The performance of lifeline utilities following the 27th February 2010 Maule Earthquake Chile," 2011.

[7] A. K. Tang, P. Eng, C. Eng, and F. Asce, "Lifelines Performance of the Mw 8.8 off Shore Biobío, Chile Earthquake," *Procedia Eng.*, vol. 14, pp. 922–930, 2011, doi: 10.1016/j.proeng.2011.07.116.

[8] EERI, "El Mayor Cucapah, Baja California Earthquake of April 4, 2010: Reconnaissance Report," Oakland, California, USA, 2010.

[9] J. Eidinger and M. Yashinsky, "Oil and water system performance – Denali M 7.9 earthquake of November 3, 2002. In: Yashinsky, M. (Ed.), 2004. San Simeon Earthquake of December 22, 2003 and Denali, Alaska, Earthquake of November 3, 2002," Reston VA, USA, 2004.

[10] D. G. Wareham and M. Bourke, "The 2010–2011 Canterbury earthquakes: impact on the liquid waste management system of Christchurch, New Zealand," *Civ. Eng. Environ. Syst.*, vol. 30, no. 1, pp. 1–14, Mar. 2013, doi: 10.1080/10286608.2012.709507.

[11] J. Eindinger, "Performance of water systems in the Mw 8.4 Atico (Perù) earthquake of June 23, 2001. In: Edwards, C.L. (Ed.), 2002. Atico, Peru, Mw 8.4 Earthquake of June 23, 2001: Lifeline Performance," 2001.

[12] J. Eindinger and A. K. Tang, "Christchurch, New Zealand Earthquake Sequence of Mw 7.1 September 04, 2010 Mw 6.3 February 22, 2011 Mw 6.0 June 13, 2011: Lifeline Performance," Reston, VA, USA, 2012.

[13] M. Erdik, "Report on 1999 Kocaeli and Düzce (Turkey) Earthquakes," 1999.

[14] A. Panico *et al.*, "Evaluating the structural priorities for the seismic vulnerability of civilian and industrial wastewater treatment plants," *Saf. Sci.*, vol. 97, pp. 51–57, Aug. 2017, doi: 10.1016/j.ssci.2015.12.030.

[15] S. Kuraoka and J. H. Rainer, "Damage to water distribution system caused by the 1995 Hyogo-ken Nanbu earthquake," *Can. J. Civ. Eng.*, vol. 23, no. 3, pp. 665–677, Jun. 1996, doi: 10.1139/l96-882.

[16] A. J. Schiff, "Hyogoken-Nanbu (Kobe), Earthquake of January 17, 1995, Lifeline Performance," 1998.

[17] A. Rodriguez-Marek, J. Williams, J. Wartman, and P. Repetto, "Ground motion and site response Southern Peru Earthquake of June 21, 2001 Reconnaissance Report," 2003.

[18] M. Yashinsky, "San Simeon Earthquake of December 22, 2003, and Denali, Alaska, Earthquake of November 3, 2002," Reston, VA, USA, 2004.

[19] NIST, "Disaster Resilience Framework (Draft)," 2014. [Online]. Available: https://www.nist.gov/system/files/documents/el/building_materials/resilience/Disaster_Resilience_Chapter_9_Water_and_Wastewater_50-Draft_102014.pdf.

[20] D. Ballantyne and C. Crouse, "Reliability and Restoration of Water Supply Systems for Fire Supression and Drinking Following Earthquakes," 1997.

[21] NIST, "The January 17, 1995 Hyogoken-Nanbu (kobe) Earthquake: Performance of Structures, Lifelines, and Fire Protection Systems," 1996.

[22] J. Meneses *et al.*, *The El Mayor Cucapah , Baja California Earthquake The El Mayor Cucapah , Exponent Failure Analysis Associates*. 2010.

[23] K. Kakderi and S. Argyroudis, "Fragility Functions of Water and Waste-Water Systems," in *Geotechnical, Geological and Earthquake Engineering*, vol. 27, 2014, pp. 221–258.

[24] A. Panico, G. Lanzano, E. Salzano, F. S. De Magistris, and G. Fabbrocino, "Seismic vulnerability of wastewater treatment plants," *Chem. Eng. Trans.*, vol. 32, no. January, pp. 13–18, 2013, doi: 10.3303/CET1332003.

[25] X. Y. Wang and A. M. Fu, "Earthquake Impact on the Sewage Treatment Plant and Emergency Measures," *Adv. Mater. Res.*, vol. 243–249, pp. 5076–5079, May 2011, doi: 10.4028/www.scientific.net/AMR.243-249.5076.

[26] M. N. Alpaslan, D. Dölgen, and H. Sarptaş, *Atıksu Arıtma Tesisleri Tasarım ve İşletme Esasları*. İzmir: Dokuz Eylül Üniversitesi Çevre Araştırma ve Uygulama Merkezi (ÇEVMER), 2004.

[27] I. Metcalf & Eddy, *Wastewater engineering : treatment and reuse*. Fourth edition / revised by George Tchobanoglous, Franklin L. Burton, H. David Stensel. Boston : McGraw-Hill, [2003] ©2003, 2003.

[28] J. H. Jung, H. S. Yoon, and C. Y. Lee, "Effect of natural frequency modes on sloshing phenomenon in a rectangular tank," *Int. J. Nav. Archit. Ocean Eng.*, vol. 7, no. 3, pp. 580–594, May 2015, doi: 10.1515/ijnaoe-2015-0041.

[29] A. VakilaadSarabi and M. Miyajima, "Study of the Sloshing of Water Reservoirs and Tanks due to Long Period and Long Duration Seismic Motions," 2012.

[30] R. Ibrahim, "LIQUID SLOSHING," S. B. T.-E. of V. Braun, Ed. Oxford: Elsevier, 2001, pp. 726–740.

[31] H. Olsen and K. R. Johnsen, "Nonlinear sloshing in rectangular tanks. A pilot study on the applicability of analytical models," 1975.

[32] O. F. Rognebakke, "Sloshing in rectangular tanks and interaction with ship motions," Norwegian University of Science and Technology, 2002.

[33] L. Ren, Y. Zou, J. Tang, X. Jin, D. Li, and M. Liu, "Numerical Modeling of Coupled Surge-Heave Sloshing in a Rectangular Tank with Baffles," *Shock Vib.*, vol. 2021, p. 5545635, 2021, doi: 10.1155/2021/5545635.

[34] P. Disimile, J. Pyles, and N. Toy, "Hydraulic Jump Formation in Water Sloshing Within an Oscillating Tank," *J. Aircr. - J Aircr.*, vol. 46, pp. 549–556, Mar. 2009, doi: 10.2514/1.38493.

[35] T. Lee, Z. Zhou, and Y. Cao, "Numerical Simulations of Hydraulic Jumps in Water Sloshing and Water Impacting ," *J. Fluids Eng.*, vol. 124, no. 1, pp. 215–226, 2001, doi: 10.1115/1.1436097.

[36] S. Gurusamy, V. S. Sanapala, D. Kumar, and B. S. V Patnaik, "Sloshing dynamics of shallow water tanks: Modal characteristics of hydraulic jumps," *J. Fluids Struct.*, vol. 104, p. 103322, 2021, doi: https://doi.org/10.1016/j.jfluidstructs.2021.103322.

[37] P. J. Disimile and N. Toy, "The imaging of fluid sloshing within a closed tank undergoing oscillations," *Results Eng.*, vol. 2, p. 100014, 2019, doi: https://doi.org/10.1016/j.rineng.2019.100014.

[38] M. Aksel, "Dairesel Tipteki Çöktürme Havuzunun Deprem Altındaki Çalkalanma Analizi," *Türk Deprem Araştırma Derg.*, vol. 3, no. 2, pp. 149–166, Dec. 2021, doi: 10.46464/tdad.1014192.

[39] P. Du *et al.*, "Environmental risk evaluation to minimize impacts within the area affected by the Wenchuan earthquake," *Sci. Total Environ.*, vol. 419, pp. 16–24, Mar. 2012, doi: 10.1016/j.scitotenv.2011.12.017.

[40] J. Lee, D. Perera, T. Glickman, and L. Taing, "Water-related disasters and their health impacts: A global review," *Prog. Disaster Sci.*, vol. 8, p. 100123, Dec. 2020, doi: 10.1016/j.pdisas.2020.100123.

[41] F. Maleki, S. Hemati, and R. Pourashraf, "Prevalence Waterborne Infections after Earthquakes Considered as Serious Threat to Increasing Victims in Disaster-Affected Areas," *Egypt. J. Vet. Sci.*, vol. 51, no. 1, pp. 111–117, Jun. 2020, doi: 10.21608/ejvs.2019.18629.1114.

[42] E. J. Nelson, J. R. Andrews, S. Maples, M. Barry, and J. D. Clemens, "Is a Cholera Outbreak Preventable in Post-earthquake Nepal?," *PLoS Negl. Trop. Dis.*, vol. 9, no. 8, p. e0003961, Aug. 2015, doi: 10.1371/journal.pntd.0003961.

[43] J. T. Watson, M. Gayer, and M. A. Connolly, "Epidemics after Natural Disasters," *Emerg. Infect. Dis.*, vol. 13, no. 1, pp. 1–5, Jan. 2007, doi: 10.3201/eid1301.060779.

[44] G. Yazici, A. K. Ö. Roglu, M. Aksel, and Y. H. Önen, "Seismic Vulnerability of Treatment Plants in Istanbul," no. May, 2015.

[45] M. R. Zare, S. Wilkinson, and R. Potangaroa, "Vulnerability of Wastewater Treatment Plants and Wastewater Pumping Stations to Earthquakes," *Int. J. Strateg. Prop. Manag.*, vol. 14, no. 4, pp. 408–420, Dec. 2010, doi: 10.3846/ijspm.2010.30.

[46] K. Pitilakis, A. Anastasiadis, K. Kakderi, S. Argyroudis, and M. Alexoudi, *Vulnerability Assessment and Risk Management of Lifelines, Infrastructures and Critical Facilities: The Case of Thessaloniki's Metropolitan Area*. 2007.

[47] FEMA, "Multi-hazard Loss Estimation Methodology (HAZUS)," 2003.

[48] M. Liu, S. Giovinazzi, R. MacGeorge, and P. Beukman, "Wastewater Network Restoration Following the Canterbury, NZ Earthquake Sequence: Turning Post-Earthquake Recovery into Resilience Enhancement," in *International Efforts in Lifeline Earthquake Engineering*, Dec. 2013, pp. 160–167, doi: 10.1061/9780784413234.021.

[49] J. E. Richardson and V. G. Panchang, "Three-Dimensional Simulation of Scour-Inducing Flow at Bridge Piers," *J. Hydraul. Eng.*, vol. 124, no. 5, pp. 530–540, May 1998, doi: 10.1061/(ASCE)0733-9429(1998)124:5(530).

[50] H. D. Smith and D. L. Foster, "Modeling of Flow Around a Cylinder Over a Scoured Bed," *J. Waterw. Port, Coastal, Ocean Eng.*, vol. 131, no. 1, pp. 14–24, Jan. 2005, doi: 10.1061/(ASCE)0733-950X(2005)131:1(14).

[51] M. Ghasemi and S. Soltani-Gerdefaramarzi, "The Scour Bridge Simulation around a Cylindrical Pier Using Flow-3D," *J. Hydrosci. Environ.*, vol. 1, no. 2, pp. 46–54, 2017, doi: 10.22111/JHE.2017.3357.

[52] S. C. Chen and S. S. Tfwala, "Performance assessment of FLOW-3D and X flow in the numerical modelling of fish-bone type fishway hydraulics," *7th IAHR Int. Symp. Hydraul. Struct. ISHS 2018*, pp. 272–282, 2018, doi: 10.15142/T3HH1J.

[53] J. Li, S. Alinaghian, D. Joksimovic, and L. Chen, "An Integrated Hydraulic and Hydrologic Modeling Approach for Roadside Bio-Retention Facilities," *Water*, vol. 12, no. 5, p. 1248, Apr. 2020, doi: 10.3390/w12051248.

[54] A. Bayon, D. Valero, R. García-Bartual, F. José Vallés-Morán, and P. A. López-Jiménez, "Performance assessment of OpenFOAM and FLOW-3D in the numerical modeling of a low Reynolds number hydraulic jump," *Environ. Model. Softw.*, vol. 80, pp. 322–335, Jun. 2016, doi: 10.1016/j.envsoft.2016.02.018.

[55] A. Najafi-Jilani, M. Z. Niri, and N. Naderi, "Simulating three dimensional wave run-up over breakwaters covered by antifer units," *Int. J. Nav. Archit. Ocean Eng.*, vol. 6, no. 2, pp. 297–306, Jun. 2014, doi: 10.2478/IJNAOE-2013-0180.

[56] A. Musa, Y. Maliki, M. Ahmad, wan sani wan nik, O. Yaakob, and K. Samo, "Numerical Simulation of Wave Flow Over the Overtopping Breakwater for Energy Conversion (OBREC) Device," *Procedia Eng.*, vol. 194, pp. 166–173, Dec. 2017, doi: 10.1016/j.proeng.2017.08.131.

[57] M. Aksel, O. Yagci, V. S. O. Kirca, E. Erdog, and N. Heidari, "A comparative analysis of coherent structures around a pile over rigid-bed and scoured-bottom," *Ocean Eng.*, vol. 226, p. 108759, Apr. 2021, doi: 10.1016/j.oceaneng.2021.108759.

[58] L. P. Martell, "Computational fluid dynamics techniques for fixed-bed biofilm systems modeling : numerical simulations and experimental characterization [en línea]," Universitat Internacional de Catalunya, 2018.

[59] M. Patziger, "Improving wastewater treatment plant performance by applying CFD models for design and operation: selected case studies," *Water Sci. Technol.*, vol. 84, no. 2, pp. 323–332, Jan. 2021, doi: 10.2166/wst.2021.019.

[60] Q. Plana, P. Lessard, and P. A. Vanrolleghem, "Dynamic grit chamber modelling: dealing with particle settling velocity distributions," *Water Sci. Technol.*, vol. 81, no. 8, pp. 1682–1699, Mar. 2020, doi: 10.2166/wst.2020.108.

[61] E. Wicklein *et al.*, "Good modelling practice in applying computational fluid dynamics for WWTP modelling.," *Water Sci. Technol. a J. Int. Assoc. Water Pollut. Res.*, vol. 73, no. 5, pp. 969–982, 2016, doi: 10.2166/wst.2015.565.

[62] C. J. Brouckaert and C. A. Buckley, "The Use of Computational Fluid Dynamics for Improving the Design and Operation of Water and Wastewater Treatment Plants," *Water Sci. Technol.*, vol. 40, no. 4–5, pp. 81–89, Aug. 1999, doi: 10.2166/wst.1999.0578.

[63] C. Ma and M. Oka, "Numerical Investigation on Sloshing Pressure for Moss-Type LNG Tank Based on Different SPH Models ." Oct. 11, 2020.

[64] S. Ransau and E. Hansen, "Numerical Simulations of Sloshing in Rectangular Tanks," Jan. 2006, doi: 10.1115/OMAE2006-92248.

[65] S. Brizzolara *et al.*, "Comparison of experimental and numerical sloshing loads in partially filled tanks," *Anal. Des. Mar. Struct. Incl. CD-ROM*, no. Lloyd 1989, pp. 13–26, 2009, doi: 10.1201/9780203874981.ch2.

[66] Flowscience, "Flow-3D User Manual." 2019.

[67] G. Wei, "A Fixed-Mesh Method for General Moving Objects in Fluid Flow," *Mod. Phys. Lett. B*, vol. 19, no. 28, pp. 1719–1722, Dec. 2005, doi: 10.1142/S021798490501030X.

[68] H. Coleman and C. Members, *ASME V&V 20-2009 Standard for Verification and Validation in Computational Fluid Dynamics and Heat Transfer (V&V20 Committee Chair and principal author)*. ASME, 2009.

[69] J. R. Merian, "Ueber die Bewegung tropfbarer Flüssigkeiten in Gefässen [On the motion of drippable liquids in containers]," 1828.

[70] O. Yagci, M. Aksel, F. Yorgun, and M. Valyrakis, "Analysis of oscillatory flow around a rigidly attached spherical particle to the bottom in a sloshing tank," in *EGU General Assembly 2022*, 2023, p. 10068, doi: 10.5194/egusphere-egu22-10068.

[71] T. Gándara, E. C. Del Barrio, M. Cruchaga, and J. Baiges, "Experimental and numerical modeling of a sloshing problem in a stepped based rectangular tank," *Phys. Fluids*, vol. 33, no. 3, p. 033111, Mar. 2021, doi: 10.1063/5.0044682.

[72] A. I. Yılmaz, "A Review of Studies on the Sloshing Effect of Liquid in Partially Filled Tank," *Journal*, no. 11, pp. 19–28, 2018.

[73] S. Jeon *et al.*, "Experimental investigation of scale effect in sloshing phenomenon," 2008.

[74] S. C. of the 28th ITTC, "Prosedure of Sloshing Model Tests," 2017.